Electronic Supplementary Information

Novel Polyoxometalate Hybrids Consisting of Copper–Lanthanide Heterometallic / Lanthanide Germanotungstate Fragments

Junwei Zhao,[a,b] Dongying Shi,[a] Lijuan Chen,[a,c,*] Yanzhou Li,[a] Pengtao Ma,[a] Jingping Wang,[a] and Jingyang Niu[a,*]

[a]Institute of Molecular and Crystal Engineering, College of Chemistry and Chemical Engineering, Henan University, Kaifeng, Henan 475004, P. R. China. [b] State Key Laboratory of Structural Chemistry, Fujian Institute of Research on the Structure of Matter, Chinese Academy of Sciences, Fuzhou, Fujian 350002, P. R. China. [c] Basic Experiment Teaching Center, Henan University, Kaifeng, Henan 475004 P. R. China. E-mail: zhaojunwei@henu.edu.cn, jyniu@henu.edu.cn,Fax: (+86) 378 3886876

Table S1 Bond valence sum (BVS) calculations of all W, Cu and Ln atoms in **1**–**6**.

The details during the course of the refinements of structures of 1-6:

Fig. S1 a) The XPS spectrum of **2** for $W4f_{7/2}$ and $W4f_{5/2}$. b) The XPS spectrum of **2** for $Cu2p_{3/2}$ and $Cu2p_{1/2}$. c) The XPS spectrum of **2** for $Tb4d_{5/2}$. d) The XPS spectrum of **3** for $W4f_{7/2}$ and $W4f_{5/2}$. e) The XPS spectrum of **3** for $Cu2p_{3/2}$ and $Cu2p_{1/2}$. f) The XPS spectrum of **3** for $Dy4d_{3/2}$. g) The XPS spectrum of **5** for $W4f_{7/2}$ and $W4f_{5/2}$. h) The XPS spectrum of **5** for $Cu2p_{3/2}$ and $Cu2p_{1/2}$. i) The XPS spectrum of **5** for $Pr3d_{5/2}$ and $Pr3d_{3/2}$. j) The XPS spectrum of **6** for $W4f_{7/2}$ and $W4f_{5/2}$. k) The XPS spectrum of **6** for $Cu2p_{3/2}$ and $Cu2p_{1/2}$. l) The XPS spectrum of **6** for $Er4d_{3/2}$.

The descriptions of the coordination geometry of the Cu^{II} and Eu^{III} cations in 1.

Fig. S2 The 3D supramolecular architecture of **1**.

The descriptions of the coordination geometry of the Cu^{II} and La^{III} cations in 4.

The descriptions of the coordination geometry of the Cu^{II} and Er^{III} cations in 6.

Fig. S3 The 2_1 helical alignment along the crystallographical *b* direction in **6**.

Fig. S4 IR spectra of **1**–**6** and $K_8Na_2[A\text{-}\alpha\text{-}GeW_9O_{34}]\cdot 25H_2O$.

Fig. S5 Magnetization as a function of the applied field recorded at 2 K.

Fig. S6 Temperature evolution of the inverse magnetic susceptibility for **1** between 35 and 300 K. The red solid line was generated from the best fit by the Curie-Weiss expression.

Fig. S7 Temperature evolution of the inverse magnetic susceptibility for **2** between 92 and 300 K. The red solid line was generated from the best fit by the Curie-Weiss expression.

Fig. S8 Temperature evolution of the inverse magnetic susceptibility for **3** between 93 and 300 K. The red solid line was generated from the best fit by the Curie-Weiss expression.

Table S1 Bond valence sum (BVS) calculations of all W, Cu and Ln atoms in **1**–**6**.

	BVS (**1**)	BVS (**2**)	BVS (**3**)	BVS (**4**)	BVS (**5**)	BVS (**6**)
Ln1	3.18	3.27	3.11	3.28	3.09	3.04
Cu1	2.06	2.07	1.92	2.19	2.11	2.17
Cu2	2.00	2.13	2.03	2.29	2.19	2.24
Cu3	2.12	2.18	2.05	2.22	2.29	2.35
Cu4	2.30	2.28	2.32	2.13	2.32	
Cu5				2.31	2.00	
Cu6					2.61	
W1	6.15	6.38	5.83	5.98	6.10	6.13
W2	6.27	6.21	6.06	6.47	6.10	6.14
W3	6.16	6.43	5.92	6.21	6.09	6.26
W4	6.05	6.48	5.86	6.01	6.06	6.05
W5	5.96	6.32	5.98	6.09	6.03	6.26
W6	6.02	6.45	5.96	6.18	5.99	6.09
W7	6.10	6.17	5.91	6.06	6.12	6.24
W8	6.18	6.42	5.98	6.51	6.26	6.17
W9	5.96	5.81	5.83	6.30	6.16	6.34
W10	6.09	6.33	5.94	6.10	6.09	6.32
W11	6.14	6.32	5.97	5.98	6.11	5.89
W12				6.03	6.05	6.19
W13				6.11	6.26	6.17
W14				6.09	6.09	6.37
W15				6.20	6.10	6.15
W16				6.02	6.05	6.31
W17				6.11	6.07	6.29
W18				6.23	6.27	6.12
W19				6.15	6.14	6.12
W20				5.83	5.94	6.26
W21				6.11	6.24	6.31
W22				6.22	6.02	6.13

The details during the course of the refinements of structures of 1-6:

Due to the large structures of **1-6** and the existence of a large amount of weight atoms, their intensity data are not very good, leading to the ADP max/min ratio of some atoms, and it is very difficult to refine these large structures, therefore, some unit-occupancy atoms have been refined isotropically and restrainedly refined.

For **1**: The ISOR instruction is used for O4, C4, O8 and O8W. The DFIX instruction is used for N8 and C8, N10 and C10, N3 and C3, N9 and C9, N7 and C7, C7 and C8. O2W-O7W, O9W, O10W, N7, N8, N10, and C7-C10 are refined isotropically. Now, there are 30 restraints were used in the refinement.

For **2**: The ISOR instruction is used for N9, N2, C4, O4, O6, O7, O17, O19, O23, O30, O32, O36, O9, O31, N5, O20, O3, O21, O34, O39, O25, N4, O30, O11, O27, O26, O35 and O40. The DFIX instruction is used for N9 and C9, N10 and C10, C3 and C4, C9 and C10, C7 and C8, N7 and C7. The DELU instruction is used for C1 and C2, C3 and C4, C5 and C6, W8 and O34. O1W-O7W, O9W, O10W, O29, N7-N10, C1, C3 and C7-C10 are refined isotropically. Now, there are 176 restraints were used in the refinement.

For **3**: The ISOR instruction is used for O20, O28, O31, O37, O41, C2, O2, O10, N9, O4, C5, O37, W2 and O29. The DFIX instruction is used for N9 and C9, N10 and C10, C7 and C8, C9 and C10，N7 and C7, N8 and C8, C3 and C4, C5 and C6. The SIMU instruction is used for C1 and C2. O2W-O7W, O24-O26, N7, N8, N10 and C7-C10 are refined isotropically. Now, there are 104 restraints were used in the refinement.

For **4**: The ISOR instruction is used for O13, O15, O28, C13, N2, O2, O6, O39, O41, O52, O25, O23, O74, O50, C9, O10, O32, Na1, C15, O29 and C10. The DFIX instruction is used for C1 and C2, C12 and N12, C7 and C8, C9 and N9，N7 and C7, C17 and N17, C15 and C16, C15 and N15, C6 and N6, Na1 and O5W, Na1 and O8W, Na1 and O4W, O5W and O7W, O4W and O5W, O4W and O6W. The DELU instruction is used for N13 and C13. O1W, O2W, O4W-O8W, O11W, O13W, O14W, C1, C2, C4, C6, C7, C11, C12, C17, C18, N1, N7, N15 and N17 are refined isotropically. Now, there are 142 restraints.

For **5**: The ISOR instruction is used for O13, O19, O20, O51, N19, C21, Cu6, C19, C8, O5, O16 and O53. The DFIX instruction is used for N21 and C21, C21 and C22, C22 and N22, C3 and C4，C13 and C14, N18 and C18, N20 and C20, Cu6 and N21, Cu6 and N20. O2W-O4W, O6W, O7W, O9W, O11W, O16W-O2OW, O64, O72, N12, N20, N21, C3, C12, C13, C16-C18 and C20 are refined isotropically. Now, there are 93 restraints were used in the refinement.

For **6**: The ISOR instruction is used for O2, O12, O13, O18, O62, Na1, O35, O37, O67, C12, O76, O17, O60, O26, N5, N10, O51, O71, O22, O28, O15, O21, O6, O3 and O62. The DFIX instruction is used for C13 and C14, C7 and C8, N14 and C14, N13 and C13, N3 and C3, Na1 and O5W, Na1 and O6W, Na1 and O2W, Na1 and O3W, O3W and O6W, O2W and O6W, O2W and O5W, O3W and O5W, W6 and O2W, N4 and C4, N12 and C12. Na1, O2W, O3W, O5W-O10W, O32, N13, N14, C3, C4, C7, C13, and C14 are refined isotropically. Now, there are 166 restraints were used in the refinement.

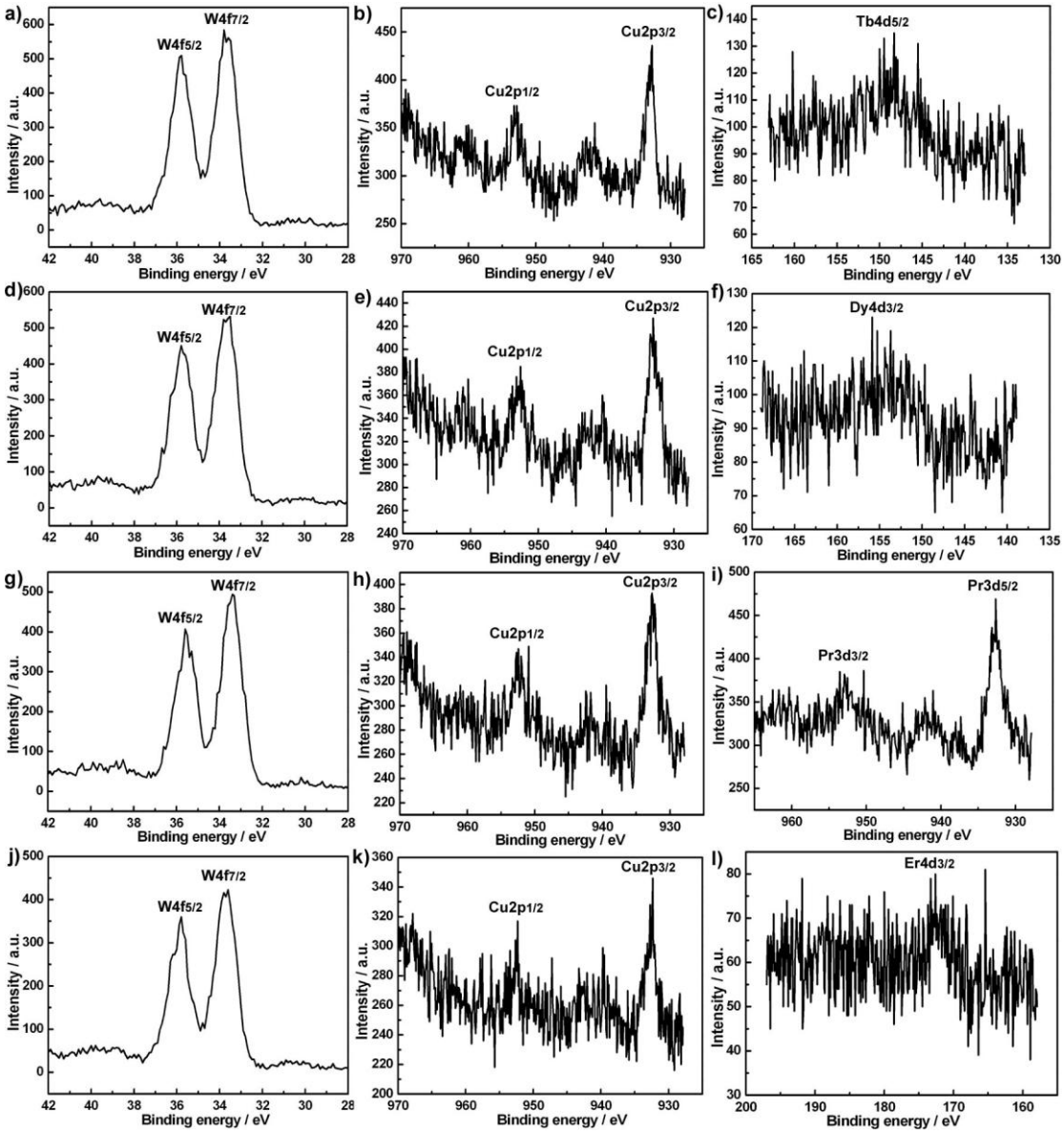

Fig. S1 a) The XPS spectrum of **2** for $W4f_{7/2}$ and $W4f_{5/2}$. b) The XPS spectrum of **2** for $Cu2p_{3/2}$ and $Cu2p_{1/2}$. c) The XPS spectrum of **2** for $Tb4d_{5/2}$. d) The XPS spectrum of **3** for $W4f_{7/2}$ and $W4f_{5/2}$. e) The XPS spectrum of **3** for $Cu2p_{3/2}$ and $Cu2p_{1/2}$. f) The XPS spectrum of **3** for $Dy4d_{3/2}$. g) The XPS spectrum of **5** for $W4f_{7/2}$ and $W4f_{5/2}$. h) The XPS spectrum of **5** for $Cu2p_{3/2}$ and $Cu2p_{1/2}$. i) The XPS spectrum of **5** for $Pr3d_{5/2}$ and $Pr3d_{3/2}$. j) The XPS spectrum of **6** for $W4f_{7/2}$ and $W4f_{5/2}$. k) The XPS spectrum of **6** for $Cu2p_{3/2}$ and $Cu2p_{1/2}$. l) The XPS spectrum of **6** for $Er4d_{3/2}$.

The descriptions of the coordination geometry of the Cu^{II} and Eu^{III} cations in 1.

In the $\{Cu_3EuO_4\}$ cubane moiety, the Cu1 and Cu2 cations inhabit in the five-coordinate square pyramidal geometry, in which the basal plane is built by two N atoms from the en ligand [Cu–N: 1.953(13)–2.038(13) Å] and two μ_3-OH groups [Cu–O: 1.972(9)–2.016(10) Å] and the vertex is occupied by a μ_4-O atom from the $[\alpha\text{-}GeW_{11}O_{39}]^{8-}$ subunit for the Cu1 cation [Cu–O: 2.598(9) Å] or a μ_3-OH group for the Cu2 cation [Cu–O: 2.273(10) Å]. The Cu3 cation adopts the six-coordinate octahedron, where two N atoms from one en ligand [Cu–N: 1.944(13)–2.009(14) Å] and two μ_3-OH ligands [Cu–O: 1.958(11)–2.017(10) Å] build the basal plane, one water O ligand

[Cu–O: 2.766(15) Å] and one μ_4-O atom from the $[\alpha\text{-}GeW_{11}O_{39}]^{8-}$ subunit [Cu–O: 2.476(9) Å] stand on two axial sites. The Eu1 cation is incorporated to the vacant site of the $[\alpha\text{-}GeW_{11}O_{39}]^{8-}$ fragment in the "cap" region and resides in an eight-coordinate distorted square antiprismatic coordination geometry (pseudo-D_{4d}) (Fig. 4d) bonding to four O atoms from the defect site of the $[\alpha\text{-}GeW_{11}O_{39}]^{8-}$ fragment [Eu–O: 2.306(11)–2.401(9) Å], to two μ_3-OH groups [Eu–O: 2.493(9) –2.515(8) Å], to one water O ligand [Eu–O: 2.434(12) Å] and to a terminal O atom from another $[\alpha\text{-}GeW_{11}O_{39}]^{8-}$ subunit [Eu–O: 2.476(10) Å]. The Eu1 cation is displaced outward and away from the normal twelfth position in the α-Keggin POM framework. In the coordination polyhedron around the Eu1 cation, the O4, O5, O6 and O7 atoms and the O1, O3, O42 and O1W atoms constitute two bottom planes of the square antiprism, and their average deviations from their least-squares planes are 0.0079 and 0.0531 Å, respectively. The dihedral angle for two bottom surfaces is1.90°. The distances between the Eu1 cation and the two bottom planes are 1.0992 and 1.4605 Å, respectively, and the ∠O–Eu–O bond angles are in the range of 57.7(3)–144.5(3) °. The above-mentioned data indicate that the square antiprism is somewhat distorted, which may be related to the coordination environments of different coordination atoms. In addition, the pendant $[Cu4(en)_2(H_2O)]^{2+}$ cation links to the $[\alpha\text{-}GeW_{11}O_{39}]^{8-}$ fragment via a terminal oxygen atom and exhibits an octahedral geometry defined by four N atoms from two en ligands [Cu–N: 1.961(19) –2.004(19) Å], a water ligand [Cu–O: 2.498(13) Å] and a terminal O atom [Cu–O: 2.658(10) Å].

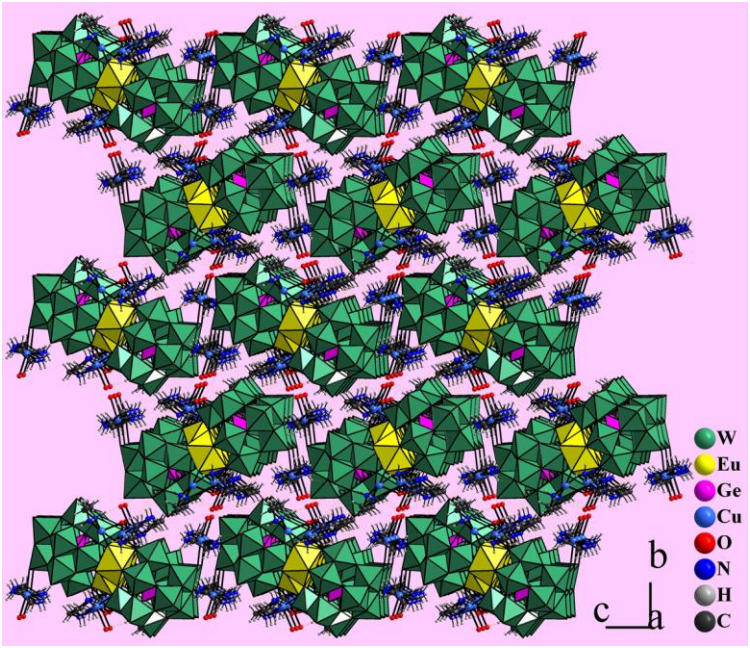

Fig. S2 The 3D supramolecular architecture of **1**.

The descriptions of the coordination geometry of the Cu^{II} and La^{III} cations in 4.

Five crystallographically independent copper cations exhibit three types of coordination geometries. The discrete $[Cu1(en)_2(H_2O)]^{2+}$, $[Cu3(en)_2(H_2O)]^{2+}$ and $[Cu4(en)_2(H_2O)]^{2+}$ cations located on the common crystallographical sites display the square pyramidal geometry with four N atoms from two en ligands [Cu–N: 1.93(3)–2.07(3) Å] and a water O ligand [Cu–O: 2.23(2)–2.486(23) Å]. The $[Cu5(en)_2(H_2O)]^{2+}$ cation standing on the common crystallographical

sites employs the planar square geometry defined by four N atoms from two en ligands [Cu–N: 1.89(2)–2.00(2) Å]. The $[Cu2(en)_2]^{2+}$ bridging cation at the special crystallographical site with the atom coordinate of (1,1,0) is six-coordinate in an octahedral geometry with four N atoms from two en ligands [Cu–N: 1.90(2)–1.95(2) Å] and two bridging O atoms from the "equatorial" W atoms on two $[\alpha\text{-}GeW_{11}O_{39}]^{8-}$ fragments [Cu–O: 2.596(16) Å]. More interestingly, the bridging functional role of the $[Cu2(en)_2]^{2+}$ cation leads to the combination of two $[La(\alpha\text{-}GeW_{11}O_{39})_2]^{13-}$ units constructing a particular tetrameric Keggin-type POM unit $\{Cu(en)_2[La(\alpha\text{-}GeW_{11}O_{39})_2]_2\}^{24-}$ (Fig. 5b). The Cu2 cation lies on the inversion center. The $[La(\alpha\text{-}GeW_{11}O_{39})_2]^{13-}$ unit is made up of an eight-coordinate square antiprismatic La^{III} cation sandwiched by two monovacant Keggin $[\alpha\text{-}GeW_{11}O_{39}]^{8-}$ fragments [La–O: 2.443(19)–2.547(18) Å], resulting in a classic sandwich-type bis(undecatungstogermanate)lanthanate structure.

The descriptions of the coordination geometry of the Cu^{II} and Er^{III} cations in 6.

There are three crystallographically unique copper-en cations (namely, $[Cu1(en)_2]^{2+}$, $[Cu2(en)_2(H_2O)]^{2+}$, and $[Cu3(en)_2]^{2+}$) in the molecular unit of **6**. It should be worth noting that the Cu1 cation is located on the inversion center of the molecular unit. The $[Cu1(en)_2]^{2+}$ and $[Cu2(en)_2(H_2O)]^{2+}$ cations are embedded in elongated octahedral geometries constituted by four N atoms [Cu–N: 1.960(15)–2.018(16) Å] and two terminal or water O atoms [Cu–O: 2.842(12)–3.181(10) Å] while the $[Cu3(en)_2]^{2+}$ cation is in the square pyramidal geometry formed by four N atoms [Cu–N: 1.960(19)–2.023(17) Å] and a terminal O atom [Cu–O: 2.533(11) Å]. The Er^{III} cation is also sandwiched by two $[\alpha\text{-}GeW_{11}O_{39}]^{8-}$ moieties showing the distorted square antiprismatic geometry with the Er–O distances of 2.321(13)–2.431(10) Å.

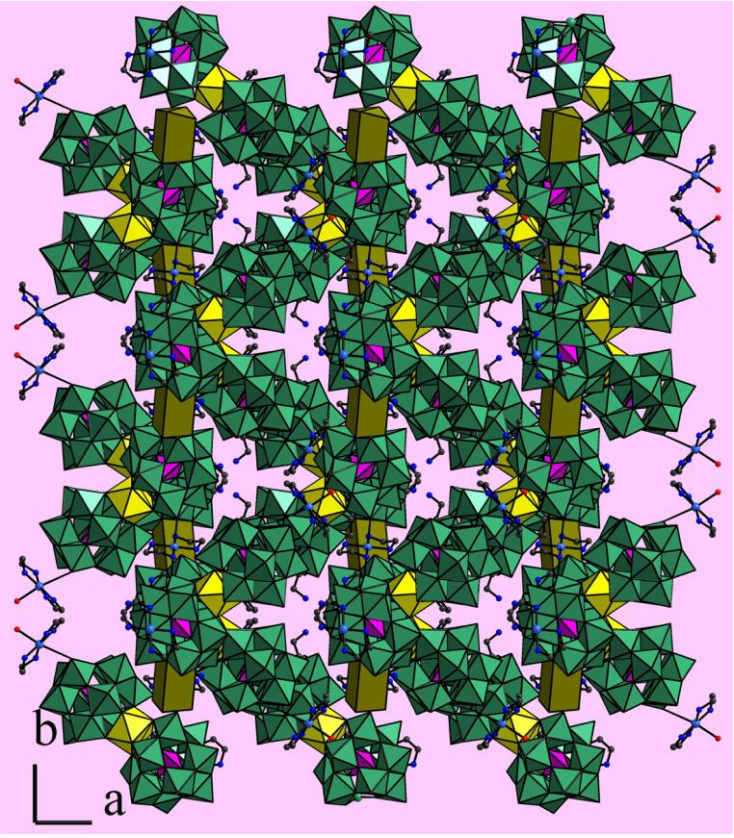

Fig. S3 The 2_1 helical alignment along the crystallographical *b* direction in **6**.

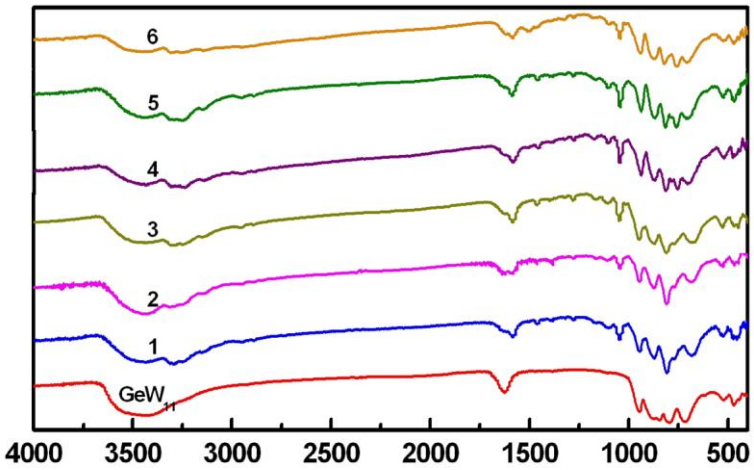

Fig. S4 IR spectra of **1**–**6** and $K_8Na_2[A\text{-}\alpha\text{-}GeW_9O_{34}]\cdot 25H_2O$.

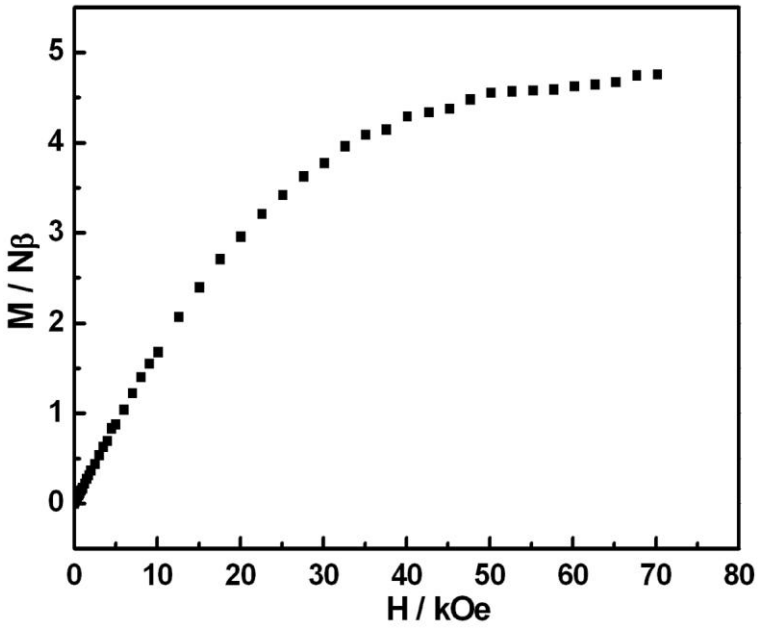

Fig. S5 Magnetization as a function of the applied field recorded at 2 K.

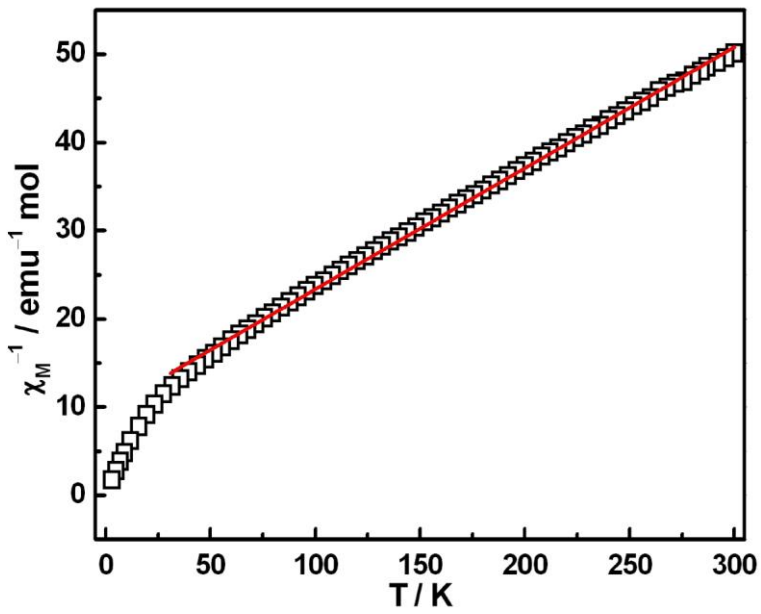

Fig. S6 Temperature evolution of the inverse magnetic susceptibility for **1** between 35 and 300 K. The red solid line was generated from the best fit by the Curie-Weiss expression.

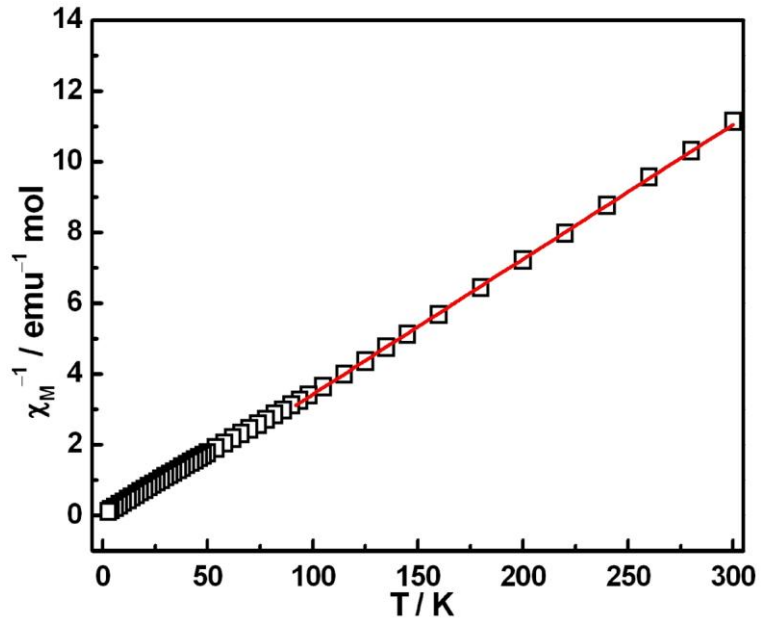

Fig. S7 Temperature evolution of the inverse magnetic susceptibility for **2** between 92 and 300 K. The red solid line was generated from the best fit by the Curie-Weiss expression.

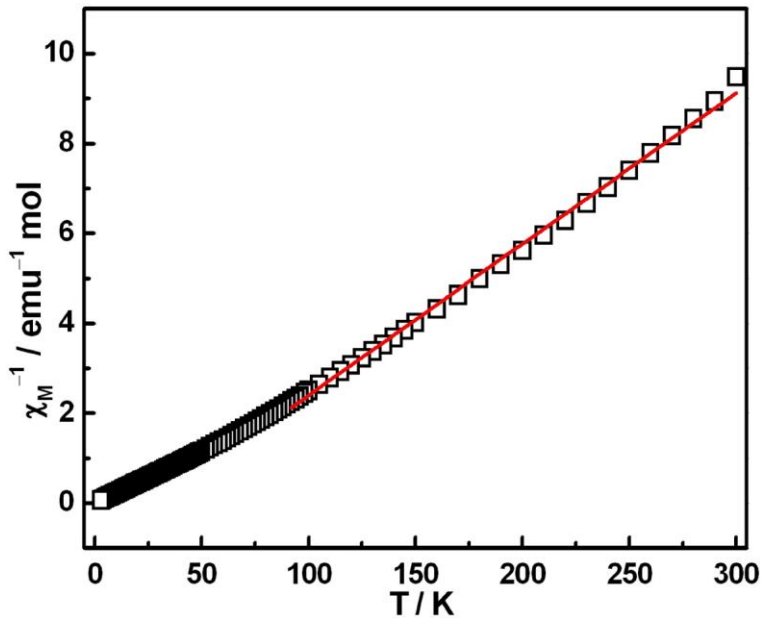

Fig. S8 Temperature evolution of the inverse magnetic susceptibility for **3** between 93 and 300 K. The red solid line was generated from the best fit by the Curie-Weiss expression.